Goblet cell LRRC26 regulates BK channel activation and protects against colitis in mice

Vivian Gonzalez-Perez[a,1], Pedro L. Martinez-Espinosa[a], Monica Sala-Rabanal[a], Nikhil Bharadwaj[a], Xiao-Ming Xia[a], Albert C. Chen[a,b], David Alvarado[c], Jenny K. Gustafsson[c,d,e], Hongzhen Hu[a], Matthew A. Ciorba[b], and Christopher J. Lingle[a]

[a]Department of Anesthesiology, Washington University School of Medicine in St. Louis, St. Louis, MO 63110; [b]McKelvey School of Engineering, Washington University in St. Louis, St. Louis, MO 63130; [c]Department of Internal Medicine, Division of Gastroenterology, Washington University School of Medicine in St. Louis, St. Louis, MO 63110; [d]Department of Medical Chemistry and Cell Biology, University of Gothenburg, 405 30 Gothenburg, Sweden; and [e]Department of Physiology, University of Gothenburg, 405 30 Gothenburg, Sweden

Edited by Richard W. Aldrich, The University of Texas at Austin, Austin, TX, and approved December 21, 2020 (received for review September 16, 2020)

Goblet cells (GCs) are specialized cells of the intestinal epithelium contributing critically to mucosal homeostasis. One of the functions of GCs is to produce and secrete MUC2, the mucin that forms the scaffold of the intestinal mucus layer coating the epithelium and separates the luminal pathogens and commensal microbiota from the host tissues. Although a variety of ion channels and transporters are thought to impact on MUC2 secretion, the specific cellular mechanisms that regulate GC function remain incompletely understood. Previously, we demonstrated that leucine-rich repeat-containing protein 26 (LRRC26), a known regulatory subunit of the Ca^{2+}-and voltage-activated K^+ channel (BK channel), localizes specifically to secretory cells within the intestinal tract. Here, utilizing a mouse model in which MUC2 is fluorescently tagged, thereby allowing visualization of single GCs in intact colonic crypts, we show that murine colonic GCs have functional LRRC26-associated BK channels. In the absence of LRRC26, BK channels are present in GCs, but are not activated at physiological conditions. In contrast, all tested $MUC2^-$ cells completely lacked BK channels. Moreover, LRRC26-associated BK channels underlie the BK channel contribution to the resting transepithelial current across mouse distal colonic mucosa. Genetic ablation of either LRRC26 or BK pore-forming α-subunit in mice results in a dramatically enhanced susceptibility to colitis induced by dextran sodium sulfate. These results demonstrate that normal potassium flux through LRRC26-associated BK channels in GCs has protective effects against colitis in mice.

LRRC26 | Ca^{2+}-activated K^+ channels | epithelial cells | DSS-induced colitis | inflammatory bowel disease

The colonic epithelium is composed of a single layer of heterogeneous cells, covered by mucus, that separate the luminal contents from host tissues. Acting both in concert and individually, the diverse cells comprising the epithelial layer play the functions of protection (1), sensation (2, 3), transport of substances (4, 5), and repair (6). Colonic epithelial cells belong to three lineages: Absorptive enterocytes, enteroendocrine cells, and goblet cells (GCs). The colonic epithelium is morphologically organized into repeating units called crypts of Lieberkühn, where stem cells located at the base of the crypts divide and successively differentiate into the mature lineages as they migrate toward the crypt surface (7). Many of the key specialized functions of epithelial cells are, in part, defined by proteins involved in ion transport, located either on their luminal or basolateral membrane. Thus, among different gastrointestinal epithelial cells, ion channels, carriers, exchangers, and pumps work in concert to define a variety of essential functions: 1) Solute and electrolyte absorption and secretion in absorptive enterocytes (reviewed in refs. 5 and 8); 2) environment sensation and serotonin secretion by enteroendocrine cells (2, 9); and 3) mucus secretion by GCs and subsequent mucus maturation into the protective layer covering the epithelial surface (10–12). Despite this progress, ionic transport in GCs and its implications in GC physiology is a topic that remains poorly understood. Here, we address the role of the Ca^{2+}- and voltage-activated K^+ channel (BK channel) in GCs.

GCs play two primary roles: One related to the maintenance of the mucosal barrier (reviewed in refs. 1 and 13) and one related with the mucosal immune homeostasis (reviewed in refs. 14 and 15). The role of GCs in barrier maintenance consists in generation of the mucus layer lining the intestinal lumen. One way GCs carry out this role is by secreting MUC2, the gel-forming mucin that forms the scaffold of the mucus layer separating luminal pathogens and commensal microbiota from the epithelial surface (11, 12, 15, 16). This separation is critical, as has been demonstrated in both animal models and humans: Mouse models with deficient mucus layer generation develop spontaneous colitis (16, 17), whereas a more penetrable mucus layer has been observed in patients with ulcerative colitis (UC), a form of human inflammatory bowel disease (IBD) (18, 19). The constant replenishment of the mucus layer involves MUC2 exocytosis from GCs, and subsequent maturation (hydration and expansion) of the secreted MUC2 to form the gel-like mucus coating the epithelium (15). Both exocytosis and maturation of MUC2 are highly dependent on anion and K^+ transport (10–12, 20). It has been proposed that mucin exocytosis in colon requires

Significance

A primary function of goblet cells (GCs) of the intestinal epithelium is to generate a protective mucus layer lining the intestinal lumen. GC dysfunction is linked to inflammatory bowel disease (IBD). GC mucus secretion is thought to be dependent on contributions of an ensemble of anion and cation fluxes, although understanding remains limited. Here, it is shown in mouse colon that the Ca^{2+}- and voltage-dependent BK-type K^+ channel, specifically in association with the LRRC26 regulatory subunit, plays a critical role in normal GC function, protecting mice against chemically induced colitis. The results demonstrate that normal K^+ fluxes mediated by LRRC26-containing BK channels are required for normal GC function, potentially providing insights into the potential role of BK channels in IBD.

Author contributions: V.G.-P., M.A.C., and C.J.L. designed research; V.G.-P., P.L.M.-E., M.S.-R., N.B., and A.C.C. performed research; X.-M.X., J.K.G., and H.H. contributed new reagents/analytic tools; V.G.-P. and D.A. analyzed data; and V.G.-P. and C.J.L. wrote the paper.

The authors declare no competing interest.

This article is a PNAS Direct Submission.

[1]To whom correspondence may be addressed. Email: gonzalezv@morpheus.wustl.edu.

This article contains supporting information online at https://www.pnas.org/lookup/suppl/doi:10.1073/pnas.2019149118/-/DCSupplemental.

Published January 11, 2021.

activities of the $Na^+/K^+/2Cl^-$ cotransporter (NKCC1) (20, 21), and also anion and K^+ channels whose identities are still unclear (20). It is also not clearly known whether specific ionic conductances are intrinsic to GCs or are located in the surrounding absorptive enterocytes. Although several types of K^+ channels—including $K_{Ca}3.1$, Kv7.1, and BK channels—have been found in colonic epithelial cells (22–27), to what extent any of those K^+ channels are specifically associated with GCs or critical to their function remains unclear. To date, most functional studies about colonic K^+ channels have focused on their roles in electrolyte and fluid secretion/absorption of the whole colon, whereas the cellular events relating K^+ channels to specific roles in GC function are still poorly understood.

Among colonic epithelial K^+ channels, the BK channel (also known as $K_{Ca}1.1$), the Ca^{2+}- and voltage-activated K^+ channel of high conductance, has been proposed to be the main component of colonic K^+ secretion into the lumen (28–30). BK channels are homotetramers of the pore-forming BKα subunit, but can also contain tissue-specific regulatory subunits that critically define the functional properties of the channel (31). BK channels composed exclusively of the pore-forming BKα subunit are unlikely to be activated at the physiological conditions of epithelial cells and, as a consequence, the molecular properties of colonic BK channels that would allow them to contribute to colonic ion transport remain unclear. Recently, we established that the leucine-rich repeat-containing protein 26 (LRRC26), a BK regulatory γ-subunit, is specifically expressed in secretory epithelial cells, including GCs of the gastrointestinal tract (32). When LRRC26 is present in a BK channel complex, the resulting channel activates near normal resting physiological conditions, even in the absence of any elevation of intracellular Ca^{2+} (33).

In the present study, we have specifically probed the role of BK channels in cells of the colonic epithelium and examined the impact of deletions of either the BKα subunit or LRRC26 on colonic function. Here, through recordings from identified GCs in intact colonic crypts, we show that LRRC26-associated BK channels contribute the major K^+ current at low intracellular Ca^{2+} (~250 nM) in mouse colonic GCs. Furthermore, the LRRC26-containing BK channels are activated near −40 mV, even in the absence of intracellular Ca^{2+}. In contrast, in identified GCs from *Lrrc26*$^{-/-}$ mice, BK current is present, but it is only activated at membrane potentials unlikely to ever occur physiologically. Surprisingly, all colonic epithelial $MUC2^-$ cells sampled completely lack functional BK channels. To establish that the LRRC26-containing BK channels contribute to normal K^+ fluxes in intact colon tissue, we show that the transepithelial current across distal colon at rest has a component dependent on LRRC26-associated BK channels, which is absent when either BKα or LRRC26 is genetically deleted. Moreover, the genetic ablation of either LRRC26 or BK channel results in a dramatically enhanced susceptibility to colitis induced by dextran sodium sulfate (DSS). Overall, our results suggest that normal potassium flux through LRRC26-associated BK channels in GCs has a protective role against development of colitis.

Results

LRRC26 Is Specifically Expressed in Epithelial GCs in Mouse Colon. The *Lrrc26*$^{-/-}$ mice, as previously described, have the entire genomic sequence of *Lrrc26* replaced with a cassette including a *LacZ* gene (32). Using the β-GAL enzymatic activity as reporter, *Lrrc26* promoter activity is primarily observed in secretory epithelial cells, including those in the gastrointestinal tract (32). Here, we examined the *Lrrc26* promoter activity in mouse colon in more detail. After incubation with X-Gal substrate, longitudinal sections of *Lrrc26*$^{-/-}$ and WT colons dissected from littermate mice identify only a subset of epithelial cells as positive for *Lrrc26* promoter activity (Fig. 1 *A* and *B* and *SI Appendix*, Fig. S1). Positive cells are found at all levels of the crypts and also in the luminal brush border surface. Positive cells in the uppermost luminal third of the crypts exhibit a morphology typical of differentiated GCs (13). The number of *Lrrc26*$^+$ cells gradually increases moving from the proximal toward the distal end of the colon, with the larger number of blue-stained cells per crypt in the two-thirds most distal segments (*SI Appendix*, Fig. S1) and the highest number per crypt in the region closer to the anorectal junction. Blue staining was not observed in lamina propria or in the smooth muscle cell layer even after varying fixation conditions or using longer substrate exposure (up to 24 h) (*SI Appendix*, Fig. S2).

At present, we are unaware of an anti-LRRC26 antibody that works for immunostaining in mouse tissues, when side-by-side comparisons between sections from WT and *Lrrc26*$^{-/-}$ mice are made. The anti-LRRC26 antibody we successfully used previously in Western blots (32) did not work in immunostainings. Therefore, in order to verify that *Lrrc26*$^+$ cells are GCs, we used X-Gal staining followed by periodic acid-Schiff (PAS) staining. PAS stains polysaccharide-rich cells and, therefore, readily identifies GC mucin granules (34). PAS is the classic method to histologically identify intestinal secretory cells which in colon are mainly GCs. X-Gal/PAS staining of frozen sections mildly fixed with either glutaraldehyde (Fig. 1 *C* and *D*) or paraformaldehyde (*SI Appendix*, Fig. S2) reveals that essentially all β-Gal$^+$ cells in the brush border or the three-quarters outermost part of the crypt were also PAS$^+$. We also observed that some PAS$^+$ cells do not show appreciable X-Gal staining. Although X-Gal staining can exhibit substantial variability (32), the basis for which is not entirely clear, the absence of staining may suggest potential heterogeneity of *Lrrc26* expression in GCs. This point is addressed below when direct recordings of LRRC26-containing BK channels in GCs are presented. It is also worthwhile to mention that a few blue-stained cells located at the base of the crypts in the most distal third of colon exhibited no appreciable PAS staining (*SI Appendix*, Fig. S2 *A* and *C*), perhaps suggesting that *Lrrc26* may also be expressed in stem cells. Overall, our results indicate that, in mouse colon, *Lrrc26* is expressed in epithelial GCs at all stages of differentiation. These results are consistent with a single-cell screening of mouse intestinal epithelial cells where *Lrrc26* has been identified as a GC marker (35).

We next examined whether knockout (KO) of LRRC26 has consequences on colonic morphology and epithelial cell composition by comparing *Lrrc26*$^{-/-}$ and WT colon histologic sections after thorough tissue fixation and staining with H&E (*SI Appendix*, Fig. S3) or PAS (Fig. 1 *E* and *F* and *SI Appendix*, Fig. S3). We analyzed the crypt metrics and GC abundance in the most distal third of colon in mice from five sets of siblings. Our results indicate that there are no substantial differences between *Lrrc26*$^{-/-}$ and WT mice in terms of crypt depth or abundance of GCs (Fig. 1 *G* and *H*). Although we observed a weak trend for *Lrrc26*$^{-/-}$ mice to have slightly shorter crypts than WT littermates (Fig. 1*G*), this difference was only marginally significant (see Fig. 1 legend for details of statistical comparison), while there was no difference in the abundance of GCs in those crypts (Fig. 1*H*).

GC BK Channels Contain LRRC26, Endowing Them with Ability to Be Activated at Resting Physiological Conditions. We have previously found that BK channels in acinar cells of lacrimal and salivary glands contain LRRC26 subunits (32). In colonic mucosa, the presence of BK channels has been documented for several species, including humans (22, 27, 30, 36, 37), although the cell types where it is expressed remain unclear. Using patch clamp, we directly tested whether colonic GCs have functional BK channels with properties consistent with the presence of LRRC26. In order to unambiguously identify the GCs, we used a transgenic mouse in which a mCherry-tag is attached to MUC2, the main

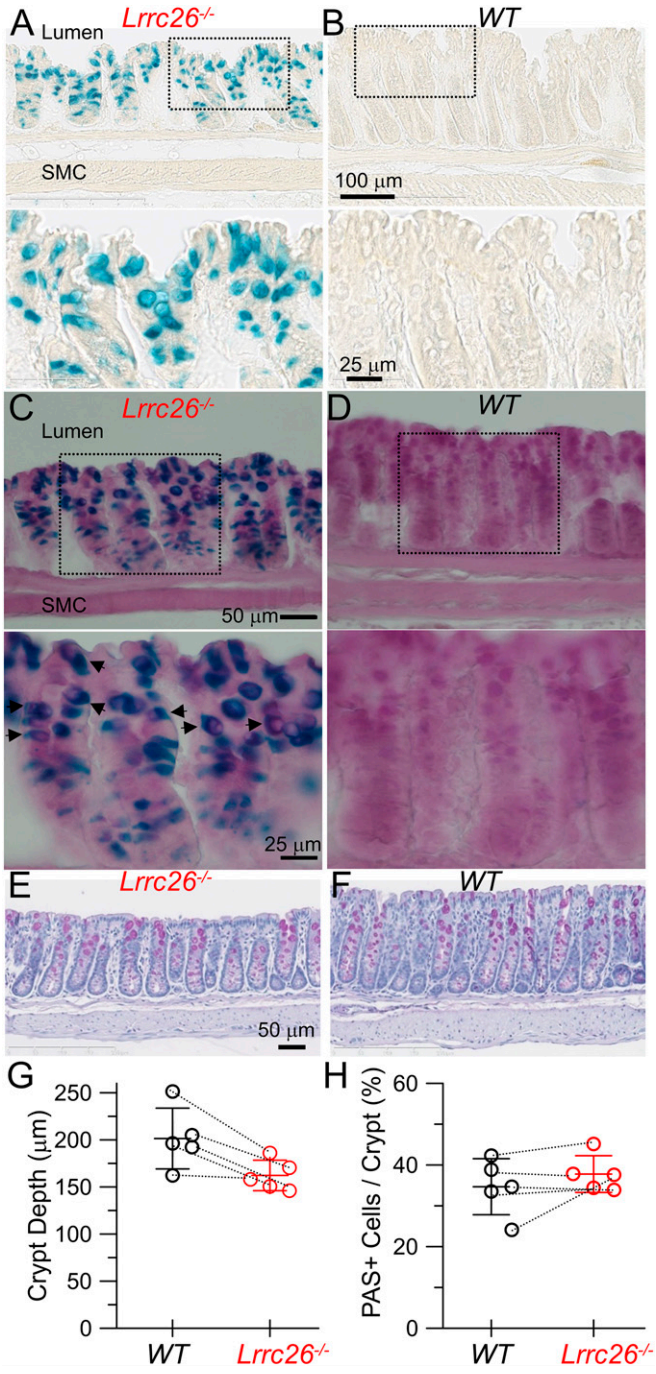

Fig. 1. In mouse colon, LRRC26 is specifically expressed in epithelial GCs. Representative images of glutaraldehyde-fixed frozen 20-μm sections of *Lrrc26*$^{-/-}$ and WT distal colons from littermates, stained side-by-side with X-Gal substrate for 1 h (*A* and *B*) or X-Gal for 1 h, followed by PAS staining (*C* and *D*). Regions outlined in the boxes (dotted lines) are shown at higher magnification below with arrowheads identifying cells positive for both *Lrrc26*-promoter activity and PAS staining. Images were taken at 0.5 cm from the anorectal junction. SMC, smooth muscle cell layer. (*E–H*) Morphological comparison between *Lrrc26*$^{-/-}$ and WT distal colon. Representative images of paraformaldehyde-fixed paraffin embedded 5-μm sections of the distal third of colons from *Lrrc26*$^{-/-}$ (*E*) and WT (*F*) littermates (taken at 1 cm from the anorectal junction), stained with PAS and counterstained with hematoxylin to identify nuclei. Comparison of crypt depth (*G*) and relative abundance of GCs per crypt (*H*) between genotypes (mean ± SD). Data plotted correspond to five sets of littermates, both sexes included, dissected at approximately same age (8 to 12 wk). In four of five sets, the litters had one WT and one *Lrrc26*$^{-/-}$, while one litter had three WTs and one *Lrrc26*$^{-/-}$. For the latter litter, the three WT siblings were averaged to obtain a single WT value plotted. Dotted lines connect results from siblings. For each animal, the value included in the plot was the average from all well-oriented crypts (at least 25) located within 4 to 20 mm from the anorectal junction. Sets of WT and *Lrrc26*$^{-/-}$ values were compared with two-tailed Student's *t* test, $P = 0.0413$ for crypt depth, $P = 0.4232$ for GC abundance.

mucin produced and secreted by gastrointestinal GCs (38). Thus, fluorescent cells are MUC2^{+}, indicative of GCs. By mating this mouse with our *Lrrc26*$^{-/-}$ mouse model, we also generated *Lrrc26*$^{-/-}$ mice with fluorescent GCs.

We recorded the whole-cell current in individual fluorescent cells of intact crypts freshly isolated from the most distal third colonic segment of WT (Fig. 2 *A* and *B*) or *Lrrc26*$^{-/-}$ mice (Fig. 2 *C* and *D*). We used solutions containing physiological Na^+ and K^+ gradients, but with glutamate replacing most of Cl^- in the solutions to minimize the contribution of anion currents, and an intracellular solution containing a Ca^{2+} concentration buffered to 250 nM, similar to conditions that we have previously utilized for patch clamping salivary gland cells (32). Our results show that, in fluorescent cells (i.e., GCs), depolarizing voltage steps evoke a time-dependent K^+ current typical of BK channels, but with a markedly shifted range of current activation between WT and *Lrrc26*$^{-/-}$ cells (Fig. 2 *B*, *D*, and *H*). In WT GCs, the K^+ current begins to be activated at a membrane potential around −40 mV with an activation curve for individual cells having, on average, a voltage of half activation of conductance (V_h) = 13.4 ± 3.2 mV.

In contrast, in *Lrrc26*$^{-/-}$ GCs, depolarizing steps up to +100 mV (red traces in Fig. 2 *B* and *D*) barely activate any K^+ current. However, further depolarization does evoke a large K^+ current, with voltage- and time-dependent activation properties characteristic of BK, with an activation *G*/*V* having on average a $V_h = 158.7 \pm 5.1$ mV for individual *Lrrc26*$^{-/-}$ GCs. Both WT and *Lrrc26*$^{-/-}$ GC-K^+ currents were pharmacologically confirmed as BK (Fig. 2 *E–G*). WT currents were reversibly blocked by bathing the cells with 5 mM tetraethyl ammonium (TEA), and both WT and *Lrrc26*$^{-/-}$ currents were completely inhibited by 200 nM of paxilline, a BK-specific blocker (39, 40). A Boltzmann fit to the averaged fractional conductance-voltage (*G-V*) curve generated from tail currents (Fig. 2*H*) yielded a V_h =13.5 mV and $z = 1.13\ e_0$ for WT-GCs, while a $V_h = 158.5$ mV and $z = 1.05\ e_0$ for *Lrrc26*$^{-/-}$ GCs. These results indicate that genetic ablation of LRRC26 results in a 145-mV rightward shift of the activation curve of GC-BK channels (Fig. 2*H*). The magnitude of the effect of LRRC26 on the activation of BK channels is consistent with the known effects of LRRC26 on heterologously expressed BK channels (41) or on native BK channels from salivary glands (32). The impact of LRRC26 is so pronounced that GC-BK channels lacking LRRC26 are hardly open and likely nonfunctional under physiological conditions. However, it is important to note that BK channels can still be identified in such *Lrrc26*$^{-/-}$ GCs, when sufficiently depolarized potentials are employed. Overall, these results indicate that mouse colonic GCs have LRRC26-associated BK channels whose gating range is suitable to permit K^+ efflux near normal physiological conditions, but only when LRR26 is present. Furthermore, the results show that BK channels are the primary K^+ current present in GCs under these conditions.

Colonic Epithelial MUC2$^-$ Cells Lack BK Channels. Next, we examined whether colonic crypt cells other than GCs have functional BK channels. Using the same preparation and ionic conditions as above, we patch-clamped nonfluorescent cells from WT mCherry-Muc2 transgenic mice. In nonfluorescent cells (i.e., MUC2$^-$ cells), which in the mouse distal colon are predominantly columnar

PHYSIOLOGY

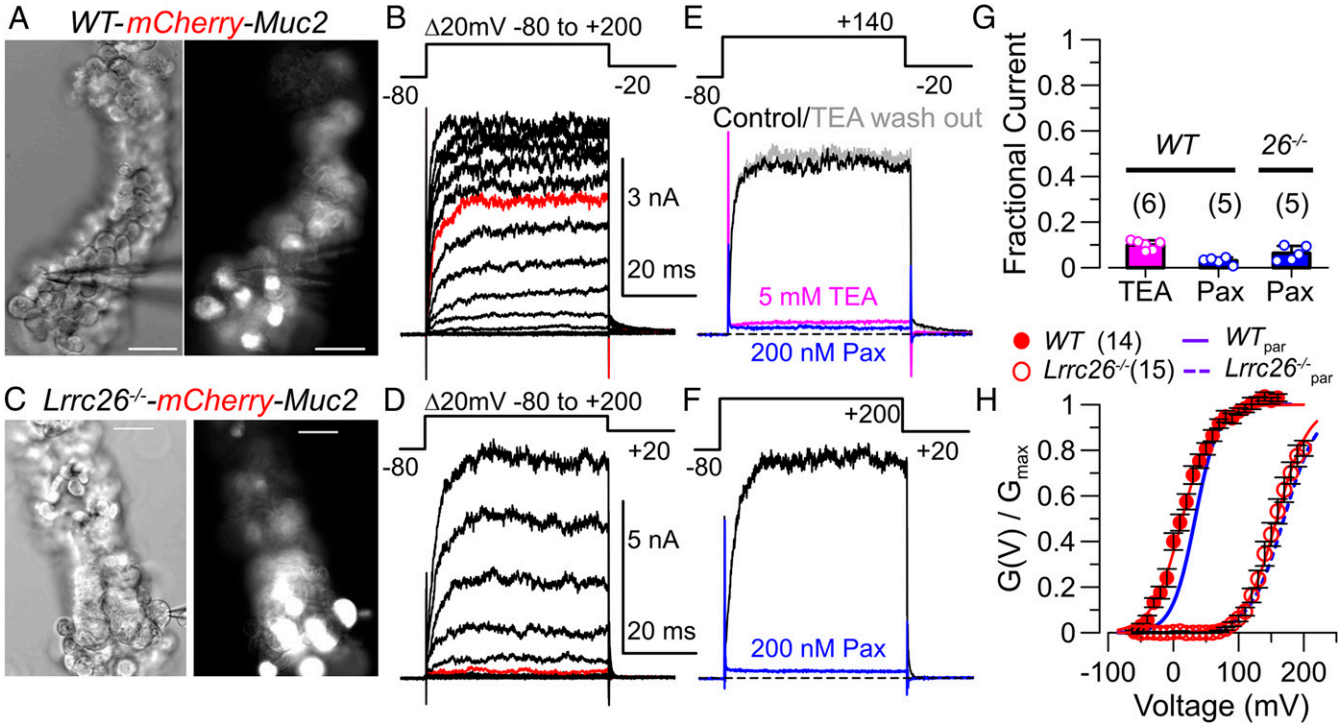

Fig. 2. BK currents in GCs exhibit properties consistent with coassembly with LRRC26 permitting channel activation at resting physiological conditions. (*A*) Brightfield and fluorescent images of a colonic crypt isolated from WT mouse (crypt oriented with opening facing downward), with the recording pipette attached to the fluorescence-identified GC whose current is shown in *B* and *E*. (Scale bars, 10 μm.) (*B*) Representative whole-cell K^+ currents evoked by the depicted voltage protocol (*Top*) in WT-GCs. (*C* and *D*) Similar experiment as in *A* and *B* performed in intact colonic crypt isolated from *Lrrc26*$^{-/-}$ mouse (scale bars, 10 μm), showing that KO of LRRC26 removes K^+ currents activated by depolarizations up to +100 mV (red traces). Dotted lines show zero current level. (*E*) K^+ current inhibition at +140 mV (maximal BK activation), in the same WT GC shown in *A* and *B*, produced by extracellular 5 mM TEA (magenta), after TEA washout (gray), and finally with 200 nM paxilline (blue). (*F*) K^+ current inhibition in the same *Lrrc26*$^{-/-}$ GC shown in *C* and *D* by 200 nM paxilline (blue). Note the much larger depolarizing step (+200 mV) required to fully activate BK current in the *Lrrc26*$^{-/-}$ GC. (*G*) Summary of pharmacological experiments confirming original current as mostly BK current (bars plot mean ± SD with points plotting measurements from individual cells). (*H*) Voltage-dependence of activation of BK conductance obtained from recordings as in *B* and *D*. Fractional conductance-voltage [$G(V)/G_{max}$] curves were generated from the tail conductances [$G(V)$], normalized to the maximum conductance (G_{max}) from a Boltzmann fit of each individual cell, and averaged (± SEM). From Boltzmann fit to individual cells, for WT GCs (n = 14), mean V_h = 13.4 ± 3.2 mV and z = 1.23 ± 0.05 e_0; for *Lrrc26*$^{-/-}$ GCs (n = 15), mean V_h = 158.7 ± 5.1 mV, and z = 1.25 ± 0.06 e_0. Fit of averaged $G(V)/G_{max}$ curves yielded similar values: WT GCs, V_h = 13.5 mV, z = 1.13 e_0; *Lrrc26*$^{-/-}$ GCs, V_h = 158.5 mV, z = 1.1. As reference, activation curves of LRRC26-associated BK or BK (lacking LRRC26) from parotid cells are shown in blue.

enterocytes, the same voltage protocol applied previously only evokes a small, time-independent current (Fig. 3 *A* and *B*) that linearly increases with the magnitude of the depolarization (Fig. 3*C*). This voltage-independent current has, on average, a reversal potential (E_{rev}) of −35.2 ± 14.4 mV (mean ± SD) for individual cells (Fig. 3*D*). The fact that, in most of MUC2$^-$ cells sampled, this current reverses at a potential apart from the theoretical K^+ reversal potential (E_{K+}) suggests that it might result from the contribution of multiple conductances (e.g., K^+-selective, Na^+-selective, or simply cation-selective). The large variability of individual E_{rev} values (Fig. 3*D*) might reflect the existence of different subsets of MUC2$^-$ cells having different sets of conductances. K^+ channels that have previously been identified in colonic epithelial cells and are potential candidates that might underlie the currents observed in MUC2$^-$ cells include K_{Ca}3.1 or Kv7.1-KCNE3 (24, 27, 42, 43). However, in only 2 of the 16 recorded nonfluorescent cells, the voltage-independent current yielded E_{rev}∼ −63 mV, suggesting a primary contribution of only a K^+-selective conductance. These two cells were located at the bottom of their respective crypts and their current showed properties similar to K_{Ca}3.1 (44).

Although further pharmacological studies are required to identify the conductances contributing to cation currents in MUC2$^-$ cells, the key point here is that such currents have no features characteristic of BK (Fig. 3 *E* and *F*). These currents lack the voltage-dependent and time-dependent activation of BK channels. Since our stimulation protocol goes up to +200 mV, it would have readily revealed the presence of BK channels, even if they lack LRRC26, over voltages from +100 to +200 mV, as seen in the *Lrrc26*$^{-/-}$ GCs. Even if only a few BK channels were present, they would have been readily detected under our recording conditions due to BK channel's large unitary conductance, which would contribute a unique increase in current variance during activation in a whole-cell recording. Unlike BK current in GCs, cation currents in MUC2$^-$ cells exhibited a significant rundown over a few minutes. Furthermore, MUC2$^-$ cells have an overall current density considerably smaller than fluorescence-identified GCs (Fig. 3*G*), despite having similar capacitance (Fig. 3*H*). The fact that none of the MUC2$^-$ cells tested (n = 16) exhibit any indication of BK current strongly suggests that colonic absorptive enterocytes not only lack LRRC26, but also lack the BKα pore-forming subunit. The finding that no BK current was observed in mouse distal colon enterocytes was surprising and contrasts with the general assumption that BK channels are widely expressed in colonic epithelial cells. However, our results are in agreement with a study in intact human crypts isolated from patient biopsies, which found BK only in a subset of nonidentified human crypt cells (27).

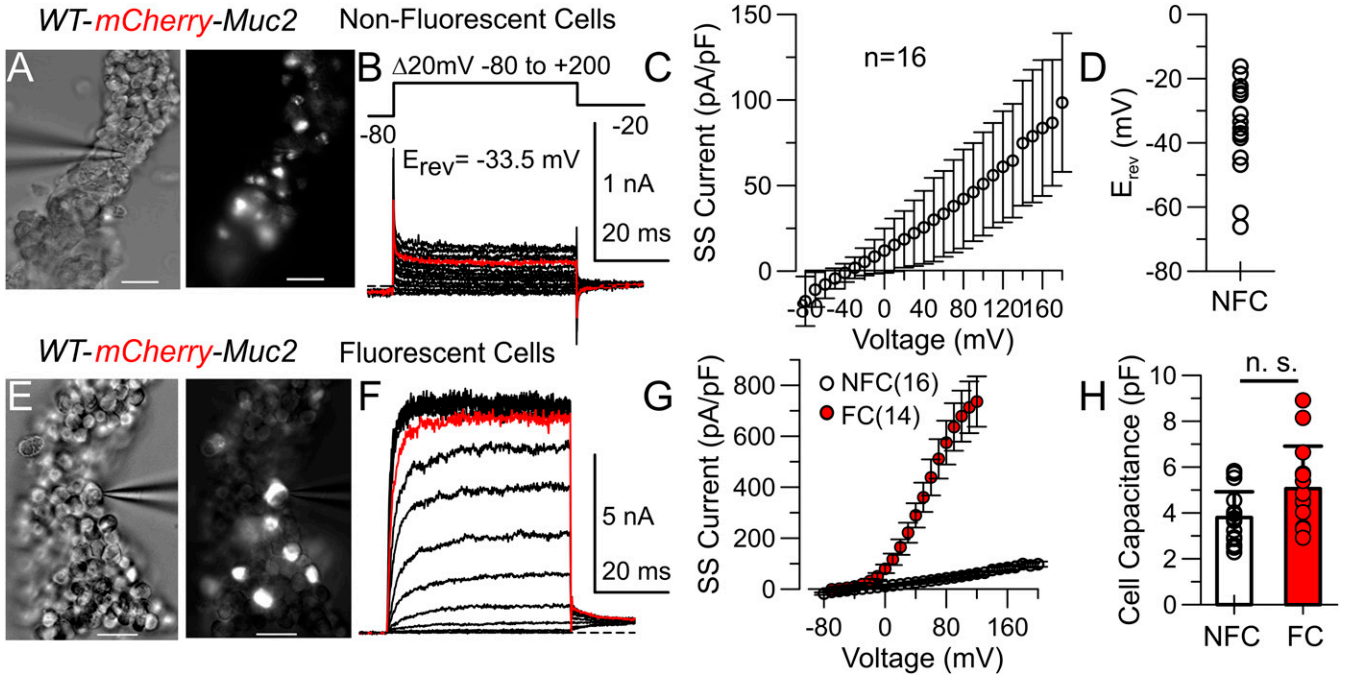

Fig. 3. Colonic epithelial MUC2$^-$ cells tested lack BK channel currents. (*A*) Brightfield and fluorescent images of colonic crypt isolated from WT mouse (opening of the crypt oriented downward), with the recording pipette attached to the nonfluorescent cell whose current is shown in *B*. (Scale bars, 10 μm.) (*B*) Representative whole-cell currents evoked by the same voltage protocol (*Top*) used in WT fluorescence-identified GCs. Red trace is the current evoked by depolarization up to +100 mV. (*C*) Voltage dependence of the whole-cell current of nonfluorescent cells (NFC) after normalization by cell capacitance. Current density at the steady-state (SS current) was calculated from current averaged during the last 10 ms of the depolarization pulse, divided by the cell capacitance, expressed as means ± SD. (*D*) Reversal potential of currents from individual NFC. (*E* and *F*) Images (scale bars, 10 μm) and representative whole-cell currents of a WT fluorescence-identified GC, showing the differences in current waveform and magnitude when compared with NFC. Note the considerable difference in amplitude reflected in the scales. (*G* and *H*) Comparison between NFC and fluorescent cells (FC) (means ± SEM) in terms of current densities (*G*) and cell capacitance (*H*). Values of current densities are significantly different at membrane potentials above −20 mV ($P < 0.001$), while capacitance values are not ($P = 0.054$), as compared by Kolmogorov–Smirnov test.

LRRC26-Associated BK Channels Contribute to Transepithelial Current under Resting Physiological Conditions. BK channels have been shown to be involved in potassium secretion in distal colon of several mammalian species (27, 30, 36, 45) and the results above demonstrate that LRRC26-containing BK channels have activation properties that would likely allow them to contribute to K^+ flux under physiological conditions. Under resting physiological conditions, Ussing chamber experiments have shown that active BK channels contribute to the net basal ionic current across distal colonic mucosa ex vivo (30, 36). This basal current is sensitive to both block of BK channels via luminal application of pharmacological agents (30, 36) or the genetic ablation of the BK α-subunit (30). Since LRRC26 uniquely defines the functionality of GC BK channels and we did not detect BK channels in MUC2$^-$ cells, we hypothesized that the contribution of BK channels to the basal transepithelial current should depend on the presence of LRRC26. Thus, genetic ablation of LRRC26 should mimic the effects of BK α-subunit KO. We therefore measured short circuit current (I_{SC}) across pieces of distal colon stripped of smooth muscle after equilibrating the tissues for 30 min in symmetrical Krebs solution. Similar to previously reported values for basal I_{SC} of mouse distal colonic mucosae (30, 46, 47), our WT tissues showed on average a basal I_{SC} = 21.6 ± 10.0 μA/cm^2 (mean ± SD, $n = 10$) (Fig. 4 *A*, *B*, and *E*). However, *Lrrc26*$^{-/-}$ mucosae showed a significantly more positive basal I_{SC} = 104.0 ± 39.5 μA/cm^2, $n = 11$ (Fig. 4 *A*, *C*, and *E*), statistically similar to I_{SC} of *BK*$^{-/-}$ tissues (basal I_{SC} = 112.6 ± 25.7 μA/cm^2, $n = 6$) (Fig. 4 *A*, *D*, and *E*), and in agreement with previously reported basal I_{SC} of *BK*$^{-/-}$ distal colonic mucosa (30).

Our results are consistent with apical LRRC26-associated BK channels underlying a basal K^+ efflux in WT tissues. Since a cationic current in the serosal-mucosal direction would contribute a negative (downward) current to the net I_{SC}, its absence in tissues lacking any of the subunits required for functionally normal GCs BK channels would lead to a more positive net basal I_{SC}. To further test this hypothesis, we examined the effects of the pharmacological block of BK channels on the basal current by luminal application of 5 mM TEA. TEA offers several advantages in terms of accessibility and kinetics of block for this type of experiment in comparison to more specific extracellular blockers of BK channels, such as Iberiotoxin (IbTx). TEA is a positively charged, highly soluble, small molecule acting as a fast blocker, and therefore does not require long exposure times characteristic of drugs such as IbTx or paxilline. Since BK channels exhibit a higher affinity for extracellular TEA (K_d ~1 mM) compared to most other K^+ channels (48, 49), the use of extracellular TEA allows a fairly specific, fast, and readily visualized effect. As predicted, 5 mM TEA induces a prompt upward change in WT basal I_{SC} that reaches a steady state within a couple of minutes (ΔI_{SC} [WT] = 19.4 ± 9.2 μA/cm^2, $n = 10$, mean ± SD) (Fig. 4 *A*, *B*, and *F*), while producing no significant change in I_{sc} of either *Lrrc26*$^{-/-}$ or BK$^{-/-}$ tissues [ΔI_{SC}(*Lrrc26*$^{-/-}$) = −3.8 ± 9.2 μA/cm^2, $n = 11$; ΔI_{SC}(*BKα*$^{-/-}$) = −2.3 ± 10.8 μA/cm^2, ($n = 6$)] (Fig. 4 *A*, *C*, *D*, and *F*). The presence of a 5 mM TEA-sensitive current under resting conditions, which is absent in both KO mouse models, supports the conclusion that LRRC26-associated BK channels of GCs underlie the K^+ secretion occurring in distal colon at resting physiological conditions.

It should be noted that the amount of I_{SC} inhibited by TEA in WT colon is less than the reduction of resting I_{SC} produced by

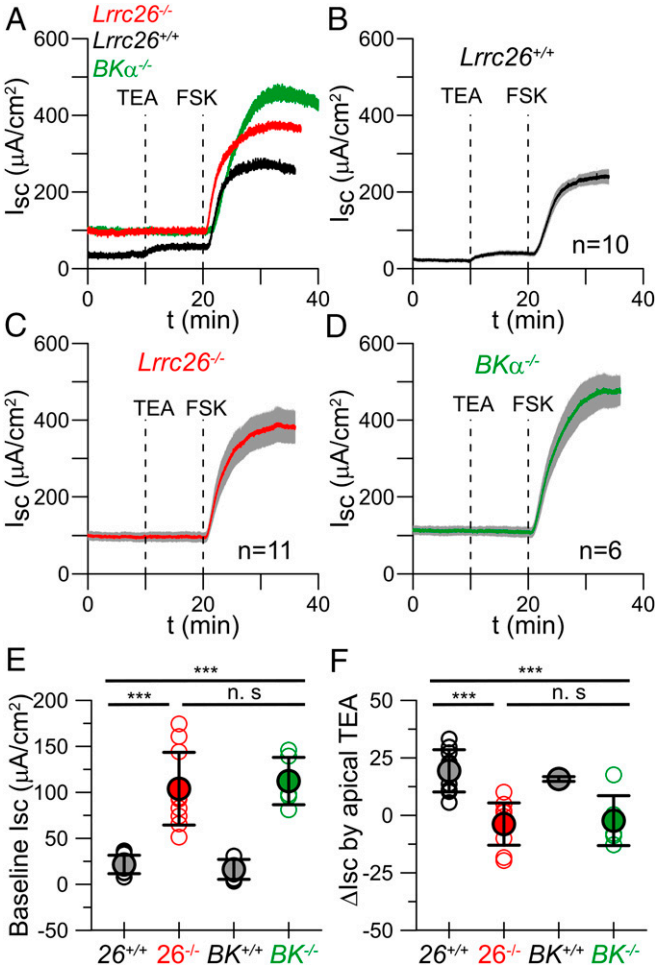

Fig. 4. LRRC26-associated BK channels contribute to the resting K^+ secretion in distal colonic mucosa. (*A*) Representative transepithelial currents (I_{SC}) recorded under voltage clamp at 0 mV in distal colonic mucosae from different genotypes. In all cases baseline I_{SC} was recorded for 10 min followed by luminal application of 5 mM TEA and 10 μM FSK at the indicated times. (*B–D*) Averaged I_{SC} (line) ± SEM (gray shadow) obtained from independent experiments for *Lrrc26*$^{-/-}$ (*B*), *Lrrc26*$^{+/+}$ (*C*), and *BK*$^{-/-}$ (*D*). (*E*) Baseline I_{SC} (mean ± SD) in the different genotypes. Sets of values were compared with ANOVA with Tukey's correction. For *Lrrc26*$^{+/+}$ vs. *Lrrc26*$^{-/-}$, $P < 0.0001$ ($n = 10$ vs. $n = 11$); for *Lrrc26*$^{+/+}$ vs. *BK*$^{-/-}$, $P < 0.0001$ ($n = 10$ vs. $n = 6$); for *Lrrc26*$^{-/-}$ vs. *BK*$^{-/-}$, $P = 0.931$ ($n = 11$ vs. $n = 6$). (*F*) Response to luminal TEA (mean ± SD). For *Lrrc26*$^{+/+}$ vs. *Lrrc26*$^{-/-}$ $P < 0.0001$ ($n = 10$ vs. $n = 11$); for *Lrrc26*$^{+/+}$ vs. *BK*$^{-/-}$, $P = 0.0004$ ($n = 10$ vs. $n = 6$); for *Lrrc26*$^{-/-}$ vs. *BK*$^{-/-}$, $P = 0.9878$ ($n = 11$ vs. $n = 6$).

either BK or LRRC26 KO. Part of the difference is expected, since 5 mM TEA will leave about 10% of GC BK current unblocked (Fig. 2 *E–G*). Another confounding factor in interpreting the absolute magnitude of both resting and evoked responses in I_{SC} experiments is that there is known up-regulation of other conductances that may occur in KO animal models. For example, it has been previously reported that *BKα*$^{-/-}$ exhibits an increased electrogenic Na^+ absorption in the distal colon in comparison with WT controls (30), which would be expected to contribute a TEA-insensitive upward component contributing to the baseline I_{SC}. This might also occur in both the *BKα*$^{-/-}$ and *Lrrc26*$^{-/-}$ models. Irrespective of any compensatory effects that might occur in both KO models that would complicate interpretation of I_{SC} measurements, the fact that a 5 mM TEA-sensitive component is equally absent in both *Lrrc26*$^{-/-}$ and *BKα*$^{-/-}$ tissues strongly suggests that the contribution of BK channels under resting conditions in colonic epithelium is mediated by BK channels containing LRRC26.

Since TEA application results in an absence of response in both KO models, to confirm viability of tissues with no obvious response we ended each experiment with the luminal application of 10 μM of the agonist forskolin (FSK). FSK induces an increase in intracellular cAMP, which elicits the activation of several conductances with the cystic fibrosis transmembrane conductance regulator (CFTR) contributing a major component (5, 8). The FSK response also likely involves contributions from multiple cell types. In all colonic strips we assayed, FSK evoked a large increase in I_{SC} as has been previously observed in mouse distal colonic strips (47, 50), thereby confirming tissue viability in cases where a TEA response was not observed. We did observe a large variability in the ΔI_{SC} induced by FSK in the presence of TEA (Fig. 4), although the measured ΔI_{SC} are not statistically different between WT and *Lrrc26*$^{-/-}$, nor between *Lrrc26*$^{-/-}$ and *BKα*$^{-/-}$, being only statistically different between WT and *BKα*$^{-/-}$ (*SI Appendix*, Fig. S4). Although the direct comparison of FSK responses among different genotypes might be informative about any potential contribution of BK channels to the cAMP-induced K^+ secretion, interpretation of the significance of the FSK responses is likely complicated by multiple factors: 1) During luminal application of TEA, any potential direct contribution of apical BK channels to the FSK response would be minimal; 2) given that apical BK contributions arise only from GCs, while the FSK response likely involves multiple cell types, any BK component in the FSK response is likely to be quite small in comparison with other components including the CFTR-mediated Cl^- flux; 3) there is the possibility of up-regulation of other conductances in both KO models that may also respond to FSK and contribute to the response. In an effort to test whether an apical BK-mediated component of the FSK response could be identified, we compared the response to FSK of the different genotypes with and without apical TEA (*SI Appendix*, Fig. S4). For all genotypes, we found no significant differences between ΔI_{SC} caused by FSK in presence or absence of TEA (*SI Appendix*, Fig. S4*G*). In addition, there were no significant difference among genotypes in ΔI_{SC} caused by FSK in the absence of TEA (*SI Appendix*, Fig. S4*G*).

Although BK channels seem to be involved in cAMP-K^+ secretion (51), given the major contribution of other conductances to the FSK-induced change in net I_{SC} from the whole mucosa, teasing apart the BK-component using this approach would require further knowledge about the individual responses of the different cell types and the use of a combination of KO mice models, together with careful pharmacological discrimination.

The Absence of LRRC26 Increases Susceptibility to DSS-Induced Colitis. Given the key role of LRRC26 in defining the functional properties of GC BK channels, we sought to investigate whether LRRC26-associated BK channel activity in GCs has implications for colonic epithelial homeostasis. Compromised intestinal epithelial homeostasis and barrier function play major roles in the development and perpetuation of the human inflammatory bowel diseases including Crohn's disease and UC (52). Although *Lrrc26*$^{-/-}$ mice exhibited no differences from WT mice in terms of gross appearance, colon histology (including crypt morphology and number of GCs) (Fig. 1 *E* and *F* and *SI Appendix*, Fig. S3), or fecal microbiota (*SI Appendix*, Fig. S5), we compared the responses of *Lrrc26*$^{-/-}$ and WT littermates in an experimental model of colitis that shares similarities to human UC, the DSS colitis model. DSS colitis is initiated by loss of epithelial barrier function with subsequent stimulation of innate and adaptive immune responses with proinflammatory cytokines that are reflective of human UC. The DSS model is typically chosen when investigations are aimed at revealing phenotypes associated with epithelial barrier function/dysfunction including

in GC function (16, 53, 54). Since our data indicate that the number of *Lrrc26*$^{+}$ GCs display a gradient increasing toward the distal colon, we chose the DSS model to challenge our *Lrrc26*$^{-/-}$ mice.

Sets of littermates were provided with drinking water containing 2.5% DSS for 7 d, and then returned to regular water. Starting on the day 5 of treatment both *Lrrc26*$^{-/-}$ and WT mice displayed a typical drop of body weight (53), accompanied by increasingly loose stools with bloody diarrhea becoming apparent around day 7. While in most WT mice the diarrhea ceased within about 24 h after switching to regular water with weight beginning to recover on day 10, in *Lrrc26*$^{-/-}$ mice bloody diarrhea and body weight loss persisted. Between days 9 and 10 a significant fraction of *Lrrc26*$^{-/-}$ mice began to show clinical signs of morbidity, including a hunched posture and inactivity to the point where they either died or required killing due to a weight loss over 30% of the initial value. By day 13 around 50% of *Lrrc26*$^{-/-}$ treated with 2.5% DSS died or required killing in comparison to <10% of WTs (Fig. 5 *A* and *B*). Increasing the DSS concentration to 3.5% DSS resulted in 100% lethality of *Lrrc26*$^{-/-}$ vs. <30% in WT littermates (Fig. 5*C*). We also compared *BKα*$^{-/-}$ and *WT* littermates using 2.5% DSS; 100% of *BKα*$^{-/-}$ mice died or required killing vs. none of WT mice (*SI Appendix*, Fig. S6). A more severe phenotype for *BKα*$^{-/-}$ mice is not unexpected, given the strong expression of BK α-subunit in nonepithelial colonic cells including the smooth muscle cell layer (30) and Cajal's cells in the lamina propria (55).

The differences in colitis severity of *Lrrc26*$^{-/-}$ vs. WT mice treated with DSS were confirmed by histology (Fig. 5 *E–H*). H&E-stained sections showed that, at day 7 of 2.5% DSS treatment, *Lrrc26*$^{-/-}$mice already have a more severe crypt and GC depletion in the distal colon in comparison with WT littermates (Fig. 5 *E*, *F*, and *I*). In addition to the crypt loss, *Lrrc26*$^{-/-}$ mice show increased inflammation (Fig. 5 *E*, *F*, and *H*), more extensive ulcerations (Fig. 5 *E*, *F*, and *H*), and larger infiltration of immune cells from the lamina propria (Fig. 5 *E* and *F*). Overall, these results demonstrate that *Lrrc26*$^{-/-}$ mice exhibit increased colitis severity and suggest a protective role for LRRC26-BK channels in the colonic epithelium.

Discussion

The present study establishes the following: 1) In colonic GCs, BK channels are associated with LRRC26 regulatory subunits and represent the major cation current present in these cells at low intracellular Ca^{2+} (~250 nM); 2) the shifted gating properties of LRRC26-containing BK channels allow them to be active at membrane potentials (−40 mV and more positive), likely to reflect normal GC resting conditions, which was also confirmed by the impact of LRRC26 KO on transepithelial ion flux measurements in intact colon strips; 3) colonic absorptive enterocytes within crypts lack BK channel currents; 4) the absence of LRRC26 in GC BK channels results in a severe DSS-induced colitis phenotype, also occurring with complete KO of the BKα subunit. The DSS-induced colitis is associated with a significantly enhanced loss of crypts and GCs in the distal colon of *Lrrc26*$^{-/-}$ in comparison to WT littermates, illustrating the importance of LRRC26 to colonic epithelial barrier function.

LRRC26 Is a Critical Component of GC BK Channels. Most existing models that summarize the interplay among different ion transport mechanisms in intestinal epithelial cells are focused on absorptive enterocytes (8, 45), whereas ion transport in GCs has been largely overlooked. There are several lines of evidence supporting the presence of BK channels in colonic epithelial cells of several species, including mice (30), rats (22, 42), guinea pigs (36), and humans (24, 27, 56), although without identifying the cell type. In rodents, colonic epithelial BK channels play a prominent role in K^{+} secretion under both basal conditions (30) and upon stimulation with purines (30), adrenaline (28), aldosterone (29, 57), or in response to high dietary K^{+} load (22, 29). However, a long unanswered question has been how these epithelial BK channels can be activated under physiological conditions. BK channels composed exclusively of the pore-forming BKα subunit would require both elevation of cytosolic Ca^{2+} to micromolar concentrations and membrane depolarizations above 0 mV in order to achieve activation necessary for its physiological roles (58). Therefore, in order for BK channels to be active under physiological conditions of colonic epithelial cells [reported to be ~120 nM intracellular Ca^{2+} at resting (59) and ~500 nM under muscarinic stimulation (60) in GCs], it seems likely that a regulatory subunit may be required.

In this study we demonstrate that the regulatory subunit LRRC26 is a critical component of BK channels in colonic GCs, allowing the BK channels to contribute to epithelial K^{+} efflux even at resting conditions. Cytosolic elevations of Ca^{2+} triggered by secretagogues or other stimuli would further enhance GC BK-mediated K^{+} fluxes. Another surprising and unexpected finding of this study concerns identification of the cell type expressing colonic epithelial BK channels. It has been suggested that epithelial BK channels fulfill their abovementioned role in K^{+} secretion by widespread expression in colonic epithelial cells, including enterocytes (8, 45). Here, we provide evidence that unambiguously indicates that, at least in mouse distal colonic epithelium, cells belonging to the GC lineage contain BK current, while BK current is absent in all MUC2^{-} cells tested. Since enterocytes are the major population of cells negative for MUC2 in distal colon, the conditions of our experiments should have readily revealed BK current in enterocytes, if it were present. In agreement with our results, previous evidence also suggests that BK channels are likely specifically expressed in GCs in human distal colon epithelium (27). Specifically, BK and $K_{Ca}3.1$ currents are the major K^{+} currents in different subsets of cells from human intact crypts (27). Although those cell types were not identified, only $K_{Ca}3.1$-containing cells developed a CFTR-mediated response to increased levels of intracellular cAMP. Therefore, the absence of a CFTR response in human crypt cells having BK currents suggests that CFTR, a protein well known to be expressed in enterocytes, and BK channels are located in different types of epithelial cells in human distal colon (27). Our evidence regarding the segregation of BK channels between distinct epithelial cell types, besides challenging previous expectations about BK cellular localization in colonic epithelium, suggests that the functional contributions of BK channels are tightly linked to the functional roles of GCs.

What Might the Role of BK Current Be in GC Function? The segregation of BK channels among colonic epithelial cells shares an interesting parallel with the previously observed probable segregation of two Ca^{2+}-dependent anion conductances, mediated by BEST2 and TMEM16A (also known as ANO1), in mouse colonic epithelium (50). In this work, Ca^{2+}-activated anion currents with properties similar to heterologously expressed BEST2 currents were the major anion current in a subset of dissociated epithelial cells presumed to be GCs. In a different set of epithelial cells, presumed to be enterocytes, the principal Ca^{2+}-activated anion current exhibited properties similar to heterologously expressed TMEM16A currents. BEST2, which has a high bicarbonate permeability relative to other anions, seems likely to be involved in the HCO_3^{-} secretion upon cholinergic stimulation (50). Besides both being specifically expressed in murine GCs, BK channels and BEST2 share a number of other features. First, both are activated by elevations of cytosolic Ca^{2+}; second, *Best2* shares with *Lrrc26* a similar increased proximal to distal gradient of expression along the colon; third, *Best2*$^{-/-}$ mice also exhibit a DSS-colitis phenotype although less severe than that occurring in *Lrrc26*$^{-/-}$ mice. One

PHYSIOLOGY

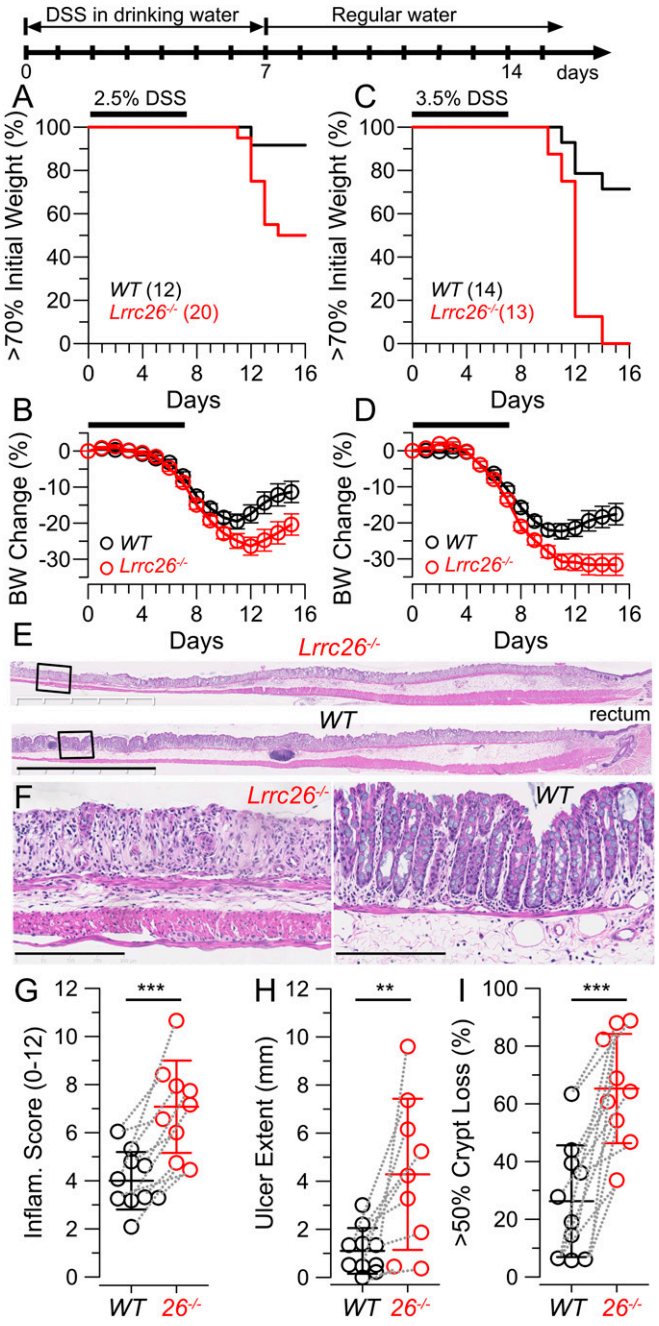

Fig. 5. Genetic ablation of LRRC26 dramatically enhances susceptibility to DSS-induced colitis. (*A–D*) Survival plots and change in body weight curves of mice treated for 7 d with 2.5% (*A* and *B*) or 3.5% DSS (MP Biomedicals, molecular mass, 36 to 50 KDa) (*C* and *D*). In accordance with guidance from Washington University in St. Louis-animal studies committee, animals whose body weight dropped >30% of their initial value were considered terminal and killed. Graphs compile results from four independent assays where eight litters (with both *Lrrc26*$^{-/-}$ and *WT* littermates) were treated with 2.5% DSS or two assays where four litters were treated with 3.5%. Mice were 10- to 14-wk old at the time of the treatment and both sexes were included. In body weight plots (mean ± SEM), for mice that died or required killing, weight at the time of death was considered the same until the end of the experiment. Curves were compared using a two-way ANOVA that yielded $P = 0.0117$ for 2.5% and $P = 0.0073$ for 3.5% DSS. (*E*) Representative images of H&E-stained most distal segment of colon from *Lrrc26*$^{-/-}$ and WT (littermates) at the day 7 of treatment. (Scale bar, 2.5 mm.) (*F*) Areas within the squares in *E*. (Scale bars, 250 μm.) (*G–I*) Histopathologic colitis severity in the distal colon of DSS-treated mice scored from sections as in *E* and *F*. Inflammation score (*G*), total ulcer extention (*H*), and fraction of epithelial surface with 50% or more of crypt loss (*I*), represented as mean ± SD. Dotted lines connect results from siblings. Sets of values were compared using two-tailed *t* test that yielded $P = 0.00054$, $P = 0.0071$, and $P = 00036$ for comparisons in *G–I*, respectively. $^{**}P < 0.01$, $^{***}P < 0.001$.

difference is that, although LRRC26-containing BK channels contribute to basal K^+ flux as revealed by the BK-dependent component of basal I_{SC}, BEST2 probably exhibits little activation until intracellular Ca^{2+} is elevated. Yet, it seems reasonable to think that a coordinated activation of K^+ flux through BK channels and bicarbonate fluxes through BEST2 channels is somehow critical in supporting mucus secretion and the extracellular conditions of Ca^{2+} and elevated pH critical to mucus expansion.

In addition to BEST2, GC BK channels might act in concert with other ion transport entities proposed to be implicated in colonic mucus secretion. For example, activation of luminal purinergic G protein-coupled (P2Y) receptors by ATP or UTP in mouse colon stimulates a K^+ secretion mediated by BK channels (30, 61). Luminal ATP stimulation also induces mucus secretion by intestinal GCs (59), which is compromised in mice with KO of TMEM16A specifically in intestinal epithelial cells. In fact, this mouse model exhibits an accumulation of mucus in intestinal GCs (59). An increase in BK channel-mediated K^+ flux during ATP-mediated mucus secretion seems plausible since the activation of P2Y receptor produces an elevation in cytosolic Ca^{2+} concentration measured in colonic GCs (59, 60). Similar mucus accumulation in GCs has also been observed in a mouse model that recapitulates a human mutation in NKCC1 (21). Both the mouse model and patients carrying this NKCC1 truncation mutation also exhibit deficient exocytosis of mucus granules from GCs, mucus attached to epithelium, and a thinner colonic mucus layer (21). Although it is not clear yet whether TMEM16A or NKCC1 influences mucus secretion by intrinsic expression in GCs or by a paracrine effect from the neighboring enterocytes, if the first case is true, K^+ flux through BK channels might act in concert with the anion transport pathways, such as NKCC1 or TMEM16A.

The demonstration here that LRRC26-containing BK channels are specifically localized in colonic GCs and contribute to resting K^+ flux in isolated colonic strips defines a component that needs to be probed in terms of how ion fluxes in GCs participate in mucus secretion and maturation. Although beyond the scope of the present work, we would suggest that LRRC26-containing BK channels may act in concert, acting as a necessary counter ion, with an anion conductance that perhaps is directly involved in the initiation of mucus exocytosis, or is critical for appropriate mucus maturation. Key questions that can now be more meaningfully pursued with respect to the role of BK and other K^+ channels in colonic function include: 1) Is there a change in mucus properties and/or mucus secretion in the *Lrrc26*$^{-/-}$ mice? 2) Is there any residual non-BK K^+ current in GCs? 3) What are the K^+ fluxes in enterocytes? Answers to these questions will allow a better understanding of the role of ion transport in colonic mucus secretion.

LRRC26-Associated BK Channels Have a Protective Effect in an Experimental Model of DSS-Induced Colitis in Mouse and Perhaps in Human IBD. Our experiments in *Lrrc26*$^{-/-}$ mice indicate that the activity of LRRC26-associated BK channels has a protective effect against colitis induced by DSS. Not surprisingly, *BKα*$^{-/-}$ mice exhibit a more profound colitis phenotype with the same treatment (Fig. 5 and *SI Appendix*, Fig. S6). These differences may be explained by the high levels of expression of BKα subunit in smooth muscle cells (30, 62), and interstitial cells of Cajal (55),

which suggest that $BK\alpha^{-/-}$ mice might also have a compromised intestinal motility.

At present, how a deficiency in K^+ flux through GC BK channels leads to enhanced susceptibility to DSS colitis remains an important unanswered question. Although it is clear that a deficit in GC BK function in $Lrrc26^{-/-}$ mice is associated with both a more drastic depletion of GCs, and a dramatically increased vulnerability to DSS in comparison to WT littermates, further studies are required to understand the cellular events underlying the protective effects of LRRC26-containing BK channels against colitis, a topic for future work.

A shared hallmark of UC and DSS-colitis is GC depletion (53, 63–65). Given the strong phenotype observed as result of genetic ablation of the subunits contributing to colonic epithelial BK channels, what are the potential implications of epithelial BK channels in human IBD? In UC patients, expression of BKα subunit in colonic crypts is enhanced (56). Whether the upregulation is an initial step in pathology, is part of a compensatory response, or involves only some or all epithelial cells are all unknown. At present, nothing is known about LRRC26 expression in UC. This is important information considering that colonic epithelial BK channels lacking LRRC26 are likely nonfunctional under physiological conditions. One might imagine that some variables, such as diet, aging, or stress-related factors could impact on LRRC26 expression, and potentially influence the susceptibility to UC. Intriguingly, work with LRRC26-containing BK channels expressed heterologously indicate that LRRC26 and BKα subunit interactions can be labile (41). Therefore, we addressed the possibility that *LRRC26* gene expression may change in different UC disease states. Analysis of a public database containing gene-expression profiles from colon of patients with IBD (66) reveals a significantly reduced expression of *LRRC26* in samples of patients with active UC in comparison to patients with inactive disease (*SI Appendix*, Fig. S7). As expected for a GC-specific protein, *LRRC26* expression positively correlates with *MUC2* expression among all samples analyzed. Consistent with having a protective role, *LRRC26* expression negatively correlates with the expression of the inflammatory cytokine IL-6 in samples of patients with active disease. These results suggest that understanding the protective role of LRRC26-associated BK channels against colitis may provide a new opportunity to understand IBD pathophysiology.

Materials and Methods

Animal Care. Animals were handled and housed according to the National Institutes of Health Committee on Laboratory Animal Resources guidelines. All experimental protocols were approved by the Institutional Animal Care and Use Committees of Washington University in St Louis (protocol #20180288). All mice were on a C57BL/6J background. The $Lrrc26^{-/-}$ mouse strain is a global KO previously described (32) and is available from the Knockout Mouse Project Repository (https://www.komp.org/) with the neomycin-resistance selection cassette deleted. The mouse referred as $BK^{-/-}$ is the $Kcnma1^{-/-}$ mouse line, a kind gift of Andrea Meredith, University of Maryland, Baltimore, MD. The mCherry-Muc2 mouse line was kindly shared by Gunnar C. Hansson, University of Gothenburg, Sweden.

X-Gal Staining. Fresh entire colons (from anus to cecum) from $Lrrc26^{-/-}$ and WT mice were dissected and rinsed with cold 0.1 M phosphate buffer, pH = 7.4 (PB). Then, colons were opened longitudinally along the mesenteric line and quickly immersion-fixed, by pinning flat with the mucosal surface facing up, in a chamber containing fixative solution, at 4 °C. The fixatives procedures were 0.2% glutaraldehyde for 24 h or 4% paraformaldehyde for 1 h, both dissolved in PB. Fixed tissues were transferred to ice-cold 30% sucrose in PB and kept at 4 °C for 48 h. Colonic pieces of 3 × 18 mm were mounted in OCT block and frozen in dry ice. Next, 20-μm frozen tissue sections were prepared in a cryostat at −20 °C. Slides were washed once briefly with 0.1 M PB and then once with 37 °C X-Gal dilution buffer (5 mM potassium ferricyanide, 5 mM potassium ferrocyanide, 2 mM magnesium chloride, 0.1% Tween-20 in PBS [pH 7.4]). Just before staining, X-Gal stock solution [4% (wt/vol) Bluo-Gal (Invitrogen, 15519-028) in dimethylformamide] was diluted at 1:40 in 37 °C X-Gal dilution buffer to prepare the fresh X-Gal working solution. Tissue sections were then incubated in the X-Gal working solution at 37 °C in a humidity box. Incubation times of 1, 2, 3, 6, 18, and 24 h were assayed. Using glutaraldehyde fixation, 1 to 2 h is enough to develop a strong and specific signal, while 3 h or longer incubation times result in unspecific signal in WT tissues. Paraformaldehyde fixed tissues requires 18 to 24 h to develop a signal. Finally, sections were rinsed in deionized water, and some sections were counterstained with PAS Staining System (395B-1KT; Sigma-Aldrich) before being mounted with aqueous mounting medium.

For quantification of the number of stained cells along colon, from distal end until the beginning of the ridges in the proximal colon, blue-stained cells per crypt were counted in five consecutive well oriented crypts, at intervals of 5 mm.

Morphological and Histological Analysis. Fresh entire colons (from anus to cecum) from $Lrrc26^{-/-}$ and WT littermates were dissected, rinsed with cold PBS, opened longitudinally along the mesenteric line, and pinned flat in a chamber containing 4% paraformaldehyde in PBS. Tissues were fixed overnight at 4 °C then transferred to 70% ethanol before processing for paraffin embedding. Five-micrometer serial sections were prepared and stained with H&E or PAS. Slide imaging was performed in a Hamamatsu Nanozoomer 2.0 HT System hosted by the Hope Center for Neurological Disorders of the Washington University in St. Louis. Morphological measurements were performed as has been previously described (67); crypt depth was quantified as the average from at least 25 well-oriented crypts per animal, all located in the distal colon at a distance between 4 and 20 mm from the anorectal junction; abundance of GCs was measured from PAS-stained tissues, and was calculated from at least 25 well-oriented crypts in the distal colon, as the percentage of GCs (stained in dark pink) regarding the total number of cells of a crypt (counting the nuclei). Colitis severity in DSS-treated mice was scored as have been described previously (67, 68).

Preparation of Crypts for Whole-Cell Recording. Intact crypts from distal colon were isolated by a modification of a Ca^{2+} chelation protocol previously reported (27, 69). Mice of 10- to 16-wk old, both sexes, were used, one mouse per day of recording. Colon was quickly dissected, rinsed with cold PBS to remove fecal content and opened longitudinally following the mesenteric line. The most distal 2 cm were cut, placed in a small glass flask containing 10 mL of Ca^{2+}-chelating solution, and incubated at 37 °C. Ca^{2+}-chelating solution was always used freshly made and contained: 20 mM Hepes, 10 mM EDTA, 112 mM NaCl, 5 mM KCl, 3 mM dithiothreitol, and adjusted to pH = 7.1 with TRIZMA base. After 3 min of incubation at 37 °C, the piece of colon was briefly and gently stirred within the solution, and further incubated at 37 °C for another 3 min. Then, after changing the piece of tissue to a new small flask containing fresh Ca^{2+}-chelating solution preincubated at 37 °C, the suspension was shaken vigorously for 3 to 4 s using a spatula, repeatedly five to six times, to liberate intact into the solution. Crypts were collected by centrifugation at 150 × *g* for 3 min at 4 °C and washed twice with cold crypt-storage solution containing: 100 mM K-gluconate, 30 mM KCl, 20 mM NaCl, 1.25 mM $CaCl_2$, 1 mM $MgCl_2$, 10 mM Hepes, 5 mM glucose, 5 mM Na-pyruvate, 5 mM Na-ubtyrate, supplemented with 1 g/L BSA, pH = 7.4 adjusted with KOH. The pellet resulting from the last centrifugation was resuspended in 0.5 mL of crypt-storage solution. 0.1 mL of the final suspension containing the crypts was seeded in coverslips (diameter 12 mm) and allowed to attach for 1 h at room temperature before beginning the patch-clamp recordings. The coverslips had been previously treated with a dilution one-tenth of Matrigel (Corning, cat #354234) in PBS for at least 30 min at 37 °C and rinsed with PBS just before seeding the crypt suspension. All experiments were obtained within 1 to 5 h after crypt dissociation.

Patch-Clamp Recordings. Standard whole-cell recording methods were done using a Multiclamp 700B amplifier (Molecular Devices). Data acquisition was performed using a 16-bit analog/digital converter and voltage stimulation protocols were accomplished by using Clampex 9.0 (Molecular Devices) with analysis of waveforms done via Clampfit. Patch-clamp pipettes were made from borosilicate glass and coated with Sylgard. Typical pipette resistances after heat-polishing typically were of 3 MΩ. Following whole-cell access, cells were used if the series resistance (R_s) was less than 10 G Ω. R_s was 90% compensated. Current records were filtered at 10 kHz. Recording solutions contained physiological gradients of Na^+ and K^+, while most of Cl^- was replaced by glutamate to minimize the contribution of any Cl^- current. The bath solution (extracellular) consisted of: 135 mM Na-glutamate, 5 mM K-glutamate, 2 mM $CaCl_2$, 2 mM $MgCl_2$, 10 mM Hepes (pH = 7.2). The pipette solution (intracellular) consisted of : 135 mM K-glutamate, 10 mM Hepes,

and 5 mM EGTA + 3 mM Ca^{2+} which results in a free Ca^{2+} solution of 250 nM (pH = 7.2). For these nominal ionic gradients, theoretical $E_K = -84.5$ mV. All the experiments were at nominal room temperature (22 to 25 °C). Tetraethylammonium (Sigma) or paxilline (Tocris Bioscience) were added (from concentrated stock solutions freshly prepared) to the extracellular solutions at final concentrations given in the text.

G-V curves of fluorescence-identified GCs were generated from the tail currents measured following a repolarization step at -20 mV for WT cells or at +20 mV for *Lrrc26*$^{-/-}$ cells. Tail current amplitude at 400 μs following the nominal repolarization step to minimize contribution of uncompensated signals. *G-V* curves were fitted to a single Boltzmann distribution:

$$G(V) = \frac{Gmax}{1 + e^{\frac{-zF(V-Vh)}{RT}}},$$

where V_h represents the voltage of half activation and z is the valence of the voltage dependence. F and R are the Faraday's and Gas's constants, respectively and T is the temperature.

Ussing Chamber Experiments. We used the most distal 2 cm of the mouse colon. After colon dissection, smooth muscle layer was removed by stripping, and a piece of mucosa was mounted in an Easy Mount Ussing chamber (Physiologic Instruments) using an insert with an aperture of 0.1 cm^2 (P2303A, Physiologic Instruments). The standard Krebs solution contained 119 mM NaCl, 2.7 mM KCl, 23 mM $NaHCO_3$, 1.25 mM Na_2HPO_4, 1.8 mM $CaCl_2$, 1.5 mM $MgSO_4$, 0.5 mM ascorbic acid, and 10 mM glucose. The reservoirs were continuously gassed with 5% CO_2 and 95% O_2 and maintained at 37 °C by water jackets. I_{SC} was measured using an automatic voltage clamping device (EVC-4000; Physiologic Instruments) that compensates for resistance of the solution between the potential measuring electrodes. The transepithelial current was applied across the tissue via a pair of Ag/AgCl electrodes that were kept in contact with the mucosal and serosal bathing solution using 3 M KCl-agar bridges. All experiments were done under voltage clamp at 0 mV. The I_{SC} is negative when positive current flows from serosa to mucosa. The tissue was placed in the apparatus and equilibrated for 30 min to stabilize I_{SC} before starting the experiment. The baseline value of electrical parameters was determined as the mean over the 10 min immediately prior to drug administration. A positive I_{SC} corresponds to the net electrogenic secretion of anions or the net electrogenic absorption of cations. FSK (10 μM) were used on the luminal side for confirming the viability of the tissues.

DSS-Induced Colitis Assay. Sets of siblings (both sexes included), 10- to 14-wk old, were treated for 7 d with drinking water containing 2.5% or 3.5% DSS (molecular mass of 36 to 50 kDa; MP Biomedicals), then switched to regular drinking water. Body weight and diarrhea score were monitored daily. Following guidelines Washington University Division of Comparative Medicine committee, mice with body weight <70% of the initial weight was considered terminal and killed. At day 7 of DSS treatment, some pairs of siblings were killed for histological comparison. Colitis severity was scored in the distal third of colons as has been described previously (67, 68), following a score (0 to 12) based on ulcer extent (0 to 4) + percent crypt loss (0 to 4) + degree of edema (0 to 4). The total ulcer extension (millimeters) and the percentage of epithelial surface with >50% of crypt loss were plotted independently.

Statistical Analysis. For comparisons between two distributions, a two-tailed unpaired Student's t test or a Kolmogorov–Smirnov test was employed. When multiple comparisons were required, an ANOVA with Tukey's correction was used. For comparison of body weight curves, a two-way ANOVA with Geisser–Greenhouse correction was used. The Geisser–Greenhouse correction was required due the lack of sphericity in the data caused by the 30% limit in the body weight drop measurements.

Data Availability. All study data are included in the article and supporting information.

ACKNOWLEDGMENTS. We thank Dr. Thaddeus Stappenbeck for useful discussions. This work was supported by the Lawrence C. Pakula, MD Inflammatory Bowel Disease Education & Innovation Fund IA-2018-10-IBD-2 (to V.G.-P.) and Grant GM-081748 (to C.J.L.). *Kcnma1* knockout mice were kindly provided by Dr. Andrea Meredith, University of Maryland, Baltimore. We acknowledge Swedish Research Council Grant 2014-00366 (to J.K.G.) and Grant 2017-00958 for the generation of the mCherry-Muc2 transgenic mouse, which was kindly provided by Dr. Gunnar C. Hansson, University of Gothenburg, Sweden. Histology services were provided by the Washington University Digestive Research Core Center supported by Grant P30DK052574. Slide imaging was performed in a Hamamatsu Nanozoomer 2.0 hosted by the Hope Center for Neurological Disorders of the Washington University in St. Louis and supported by NIH shared Instrumentation Grant S10RR027552. Microbiota analysis was performed at the Washington University Genome Technology Access Center, which is partially supported by National Cancer Institute Cancer Center Support Grant P30 CA91842 and by Institute of Clinical and Translational Sciences/Clinical and Translational Science Award Grant UL1TR000448 from the National Center for Research Resources.

1. M. E. Johansson, G. C. Hansson, Mucus and the goblet cell. *Dig. Dis.* **31**, 305–309 (2013).
2. C. Alcaino *et al*., A population of gut epithelial enterochromaffin cells is mechanosensitive and requires Piezo2 to convert force into serotonin release. *Proc. Natl. Acad. Sci. U.S.A.* **115**, E7632–E7641 (2018).
3. K. A. Knoop, K. G. McDonald, S. McCrate, J. R. McDole, R. D. Newberry, Microbial sensing by goblet cells controls immune surveillance of luminal antigens in the colon. *Mucosal Immunol.* **8**, 198–210 (2015).
4. N. Shashikanth *et al*., Epithelial organization: The gut and beyond. *Compr. Physiol.* **7**, 1497–1518 (2017).
5. K. Kunzelmann, M. Mall, Electrolyte transport in the mammalian colon: Mechanisms and implications for disease. *Physiol. Rev.* **82**, 245–289 (2002).
6. Y. Wang *et al*., Long-term culture captures injury-repair cycles of colonic stem cells. *Cell* **179**, 1144–1159.e15 (2019).
7. R. S. Sellers, D. Morton, The colon: From banal to brilliant. *Toxicol. Pathol.* **42**, 67–81 (2014).
8. D. Heitzmann, R. Warth, Physiology and pathophysiology of potassium channels in gastrointestinal epithelia. *Physiol. Rev.* **88**, 1119–1182 (2008).
9. P. R. Strege *et al*., Sodium channel $Na_V1.3$ is important for enterochromaffin cell excitability and serotonin release. *Sci. Rep.* **7**, 15650 (2017).
10. J. K. Gustafsson *et al*., Bicarbonate and functional CFTR channel are required for proper mucin secretion and link cystic fibrosis with its mucus phenotype. *J. Exp. Med.* **209**, 1263–1272 (2012).
11. D. Ambort *et al*., Calcium and pH-dependent packing and release of the gel-forming MUC2 mucin. *Proc. Natl. Acad. Sci. U.S.A.* **109**, 5645–5650 (2012).
12. A. Schütte *et al*., Microbial-induced meprin β cleavage in MUC2 mucin and a functional CFTR channel are required to release anchored small intestinal mucus. *Proc. Natl. Acad. Sci. U.S.A.* **111**, 12396–12401 (2014).
13. G. M. Birchenough, M. E. Johansson, J. K. Gustafsson, J. H. Bergström, G. C. Hansson, New developments in goblet cell mucus secretion and function. *Mucosal Immunol.* **8**, 712–719 (2015).
14. K. A. Knoop, R. D. Newberry, Goblet cells: Multifaceted players in immunity at mucosal surfaces. *Mucosal Immunol.* **11**, 1551–1557 (2018).
15. M. E. Johansson, G. C. Hansson, Immunological aspects of intestinal mucus and mucins. *Nat. Rev. Immunol.* **16**, 639–649 (2016).
16. M. Van der Sluis *et al*., Muc2-deficient mice spontaneously develop colitis, indicating that MUC2 is critical for colonic protection. *Gastroenterology* **131**, 117–129 (2006).
17. A. M. Robinson *et al*., Alterations of colonic function in the Winnie mouse model of spontaneous chronic colitis. *Am. J. Physiol. Gastrointest. Liver Physiol.* **312**, G85–G102 (2017).
18. M. E. Johansson *et al*., Bacteria penetrate the normally impenetrable inner colon mucus layer in both murine colitis models and patients with ulcerative colitis. *Gut* **63**, 281–291 (2014).
19. J. K. Gustafsson *et al*., An ex vivo method for studying mucus formation, properties, and thickness in human colonic biopsies and mouse small and large intestinal explants. *Am. J. Physiol. Gastrointest. Liver Physiol.* **302**, G430–G438 (2012).
20. J. K. Gustafsson *et al*., Carbachol-induced colonic mucus formation requires transport via NKCC1, K^+ channels and CFTR. *Pflugers Arch.* **467**, 1403–1415 (2015).
21. R. Koumangoye, S. Omer, M. H. Kabeer, E. Delpire, Novel human NKCC1 mutations cause defects in goblet cell mucus secretion and chronic inflammation. *Cell. Mol. Gastroenterol. Hepatol.* **9**, 239–255 (2020).
22. I. Butterfield, G. Warhurst, M. N. Jones, G. I. Sandle, Characterization of apical potassium channels induced in rat distal colon during potassium adaptation. *J. Physiol.* **501**, 537–547 (1997).
23. R. B. Lomax, G. Warhurst, G. I. Sandle, Characteristics of two basolateral potassium channel populations in human colonic crypts. *Gut* **38**, 243–247 (1996).
24. G. I. Sandle, C. M. McNicholas, R. B. Lomax, Potassium channels in colonic crypts. *Lancet* **343**, 23–25 (1994).
25. B. C. Schroeder *et al*., A constitutively open potassium channel formed by KCNQ1 and KCNE3. *Nature* **403**, 196–199 (2000).
26. F. Julio-Kalajzić *et al*., K_{2P} TASK-2 and KCNQ1-KCNE3 K^+ channels are major players contributing to intestinal anion and fluid secretion. *J. Physiol.* **596**, 393–407 (2018).
27. J. Linley, A. Loganathan, S. Kopanati, G. I. Sandle, M. Hunter, Evidence that two distinct crypt cell types secrete chloride and potassium in human colon. *Gut* **63**, 472–479 (2014).
28. M. V. Sørensen *et al*., Adrenaline-induced colonic K+ secretion is mediated by KCa1.1 (BK) channels. *J. Physiol.* **588**, 1763–1777 (2010).
29. M. V. Sørensen *et al*., Aldosterone increases KCa1.1 (BK) channel-mediated colonic K+ secretion. *J. Physiol.* **586**, 4251–4264 (2008).
30. M. Sausbier *et al*., Distal colonic K(+) secretion occurs via BK channels. *J. Am. Soc. Nephrol.* **17**, 1275–1282 (2006).

31. V. Gonzalez-Perez, C. J. Lingle, Regulation of BK channels by beta and gamma subunits. *Annu. Rev. Physiol.* **81**, 113–137 (2019).
32. C. Yang *et al*., Knockout of the LRRC26 subunit reveals a primary role of LRRC26-containing BK channels in secretory epithelial cells. *Proc. Natl. Acad. Sci. U.S.A.* **114**, E3739–E3747 (2017).
33. J. Yan, R. W. Aldrich, LRRC26 auxiliary protein allows BK channel activation at resting voltage without calcium. *Nature* **466**, 513–516 (2010).
34. M. Mantle, A. Allen, A colorimetric assay for glycoproteins based on the periodic acid/Schiff stain [proceedings]. *Biochem. Soc. Trans.* **6**, 607–609 (1978).
35. A. L. Haber *et al*., A single-cell survey of the small intestinal epithelium. *Nature* **551**, 333–339 (2017).
36. J. Zhang, S. T. Halm, D. R. Halm, Role of the BK channel (KCa1.1) during activation of electrogenic K+ secretion in guinea pig distal colon. *Am. J. Physiol. Gastrointest. Liver Physiol.* **303**, G1322–G1334 (2012).
37. G. I. Sandle, M. Hunter, Apical potassium (BK) channels and enhanced potassium secretion in human colon. *QJM* **103**, 85–89 (2010).
38. G. M. Birchenough, E. E. Nyström, M. E. Johansson, G. C. Hansson, A sentinel goblet cell guards the colonic crypt by triggering Nlrp6-dependent Muc2 secretion. *Science* **352**, 1535–1542 (2016).
39. W. L. Imlach *et al*., The molecular mechanism of "ryegrass staggers," a neurological disorder of K+ channels. *J. Pharmacol. Exp. Ther.* **327**, 657–664 (2008).
40. Y. Zhou, C. J. Lingle, Paxilline inhibits BK channels by an almost exclusively closed-channel block mechanism. *J. Gen. Physiol.* **144**, 415–440 (2014).
41. V. Gonzalez-Perez, X. M. Xia, C. J. Lingle, Functional regulation of BK potassium channels by γ1 auxiliary subunits. *Proc. Natl. Acad. Sci. U.S.A.* **111**, 4868–4873 (2014).
42. B. C. Burckhardt, H. Gögelein, Small and maxi K+ channels in the basolateral membrane of isolated crypts from rat distal colon: Single-channel and slow whole-cell recordings. *Pflugers Arch.* **420**, 54–60 (1992).
43. P. Preston *et al*., Disruption of the K+ channel beta-subunit KCNE3 reveals an important role in intestinal and tracheal Cl- transport. *J. Biol. Chem.* **285**, 7165–7175 (2010).
44. W. J. Joiner, L.-Y. Wang, M. D. Tang, L. K. Kaczmarek, hSK4, a member of a novel subfamily of calcium-activated potassium channels. *Proc. Natl. Acad. Sci. U.S.A.* **94**, 11013–11018 (1997).
45. V. M. Rajendran, G. I. Sandle, Colonic potassium absorption and secretion in health and disease. *Compr. Physiol.* **8**, 1513–1536 (2018).
46. H. C. Hartzell, Z. Qu, K. Yu, Q. Xiao, L. T. Chien, Molecular physiology of bestrophins: Multifunctional membrane proteins linked to best disease and other retinopathies. *Physiol. Rev.* **88**, 639–672 (2008).
47. T. S. Rottgen *et al*., Dextran sulfate sodium-induced chronic colitis attenuates Ca^{2+}-activated Cl^- secretion in murine colon by downregulating TMEM16A. *Am. J. Physiol. Cell Physiol.* **315**, C10–C20 (2018).
48. C. Vergara, E. Moczydlowski, R. Latorre, Conduction, blockade and gating in a Ca-activated K channel incorporated into planar lipid bilayers. *Biophys. J.* **45**, 73–76 (1984).
49. M. P. Kavanaugh *et al*., Interaction between tetraethylammonium and amino acid residues in the pore of cloned voltage-dependent potassium channels. *J. Biol. Chem.* **266**, 7583–7587 (1991).
50. K. Yu, R. Lujan, A. Marmorstein, S. Gabriel, H. C. Hartzell, Bestrophin-2 mediates bicarbonate transport by goblet cells in mouse colon. *J. Clin. Invest.* **120**, 1722–1735 (2010).
51. G. I. Sandle, V. M. Rajendran, Cyclic AMP-induced K+ secretion occurs independently of Cl- secretion in rat distal colon. *Am. J. Physiol. Cell Physiol.* **303**, C328–C333 (2012).
52. E. Martini, S. M. Krug, B. Siegmund, M. F. Neurath, C. Becker, Mend your fences: The epithelial barrier and its relationship with mucosal immunity in inflammatory bowel disease. *Cell. Mol. Gastroenterol. Hepatol.* **4**, 33–46 (2017).
53. S. Wirtz *et al*., Chemically induced mouse models of acute and chronic intestinal inflammation. *Nat. Protoc.* **12**, 1295–1309 (2017).
54. P. Kiesler, I. J. Fuss, W. Strober, Experimental models of inflammatory bowel diseases. *Cell. Mol. Gastroenterol. Hepatol.* **1**, 154–170 (2015).
55. Y. Zhu, A. Mucci, J. D. Huizinga, Inwardly rectifying chloride channel activity in intestinal pacemaker cells. *Am. J. Physiol. Gastrointest. Liver Physiol.* **288**, G809–G821 (2005).
56. G. I. Sandle *et al*., Altered cryptal expression of luminal potassium (BK) channels in ulcerative colitis. *J. Pathol.* **212**, 66–73 (2007).
57. R. B. Lomax, C. M. McNicholas, M. Lombès, G. I. Sandle, Aldosterone-induced apical Na+ and K+ conductances are located predominantly in surface cells in rat distal colon. *Am. J. Physiol.* **266**, G71–G82 (1994).
58. D. H. Cox, J. Cui, R. W. Aldrich, Allosteric gating of a large conductance Ca-activated K+ channel. *J. Gen. Physiol.* **110**, 257–281 (1997).
59. R. Benedetto, I. Cabrita, R. Schreiber, K. Kunzelmann, TMEM16A is indispensable for basal mucus secretion in airways and intestine. *FASEB J.* **33**, 4502–4512 (2019).
60. R. Schreiber *et al*., Anoctamins support calcium-dependent chloride secretion by facilitating calcium signaling in adult mouse intestine. *Pflugers Arch.* **467**, 1203–1213 (2015).
61. J. E. Matos, B. Robaye, J. M. Boeynaems, R. Beauwens, J. Leipziger, K+ secretion activated by luminal P2Y2 and P2Y4 receptors in mouse colon. *J. Physiol.* **564**, 269–279 (2005).
62. O. Bayguinov, B. Hagen, J. L. Kenyon, K. M. Sanders, Coupling strength between localized Ca(2+) transients and K(+) channels is regulated by protein kinase C. *Am. J. Physiol. Cell Physiol.* **281**, C1512–C1523 (2001).
63. B. Chassaing, J. D. Aitken, M. Malleshappa, M. Vijay-Kumar, Dextran sulfate sodium (DSS)-induced colitis in mice. *Curr. Protoc. Immunol.* **104**, 15.25.11–15.25.14 (2014).
64. R. M. Feakins; British Society of Gastroenterology, Inflammatory bowel disease biopsies: Updated British society of gastroenterology reporting guidelines. *J. Clin. Pathol.* **66**, 1005–1026 (2013).
65. D. A. McCormick, L. W. Horton, A. S. Mee, Mucin depletion in inflammatory bowel disease. *J. Clin. Pathol.* **43**, 143–146 (1990).
66. M. Vancamelbeke *et al*., Genetic and transcriptomic bases of intestinal epithelial barrier dysfunction in inflammatory bowel disease. *Inflamm. Bowel Dis.* **23**, 1718–1729 (2017).
67. D. M. Alvarado *et al*., Epithelial indoleamine 2,3-dioxygenase 1 modulates aryl hydrocarbon receptor and notch signaling to increase differentiation of secretory cells and alter mucus-associated microbiota. *Gastroenterology* **157**, 1093–1108.e11 (2019).
68. M. A. Ciorba *et al*., Induction of IDO-1 by immunostimulatory DNA limits severity of experimental colitis. *J. Immunol.* **184**, 3907–3916 (2010).
69. K. A. Bowley, M. J. Morton, M. Hunter, G. I. Sandle, Non-genomic regulation of intermediate conductance potassium channels by aldosterone in human colonic crypt cells. *Gut* **52**, 854–860 (2003).